FREE INTERNET ROWING MODEL (FIRM)

EXAMPLES: Fours

March 25, 2015

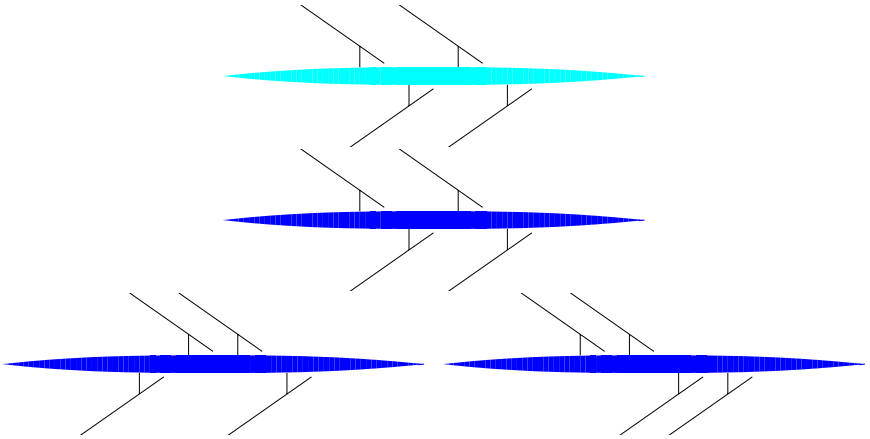

FIRM IS RESEARCH CODE!

Please check all estimates generated by the program against experimental results before committing any time or funds to your project as no liability can be accepted by Cyberiad.

Contents

1 INTRODUCTION

Five examples of rowing fours are included in this version of FIRM. More will be added in future versions.

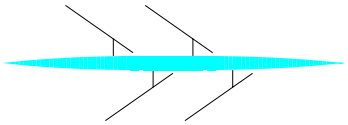

2 LM4-: Lightweight Men's Four (Normal Rig)

The on-water trial for this lightweight men's four, "Hui", "Iggy", "Jie" and "Kang", was conducted over 500m on a late spring morning. Air and water temperatures were not recorded: they were estimated as 11°C and 11°C respectively. Measured values of rigging details, oar angles, gate normal forces, and their anthropometry were used as input to FIRM. Body angle regimes were not recorded but were estimated by the author using a complicated fitting process.

Table 1: Summary of experimental results for this simulation: number of strokes, stroke rate, non-dimensional pull phase duration (t_p/t_s), minimum hull velocity (U_{min}), maximum hull velocity (U_{max}), and mean hull velocity ($\overline{U}$).

Item	Value
Nstrokes	36
Rate (spm)	37.070 ±0.248
t_p/t_s	0.476 ±0.013
U_{min} (ms^{-1})	4.243 ±0.104
U_{max} (ms^{-1})	6.869 ±0.120
$\overline{U}$ (ms^{-1})	5.809 ±0.118

Table 1 summarises the main quantities relating to the simulation for this crew. Values are given ± one standard deviation.

Table 2: Experimental oar-related values for this simulation: Minimum and maximum oar angles, and maximum gate normal force.

Name	Port Oar			Starboard Oar		
	Min. Angle (degrees)	Max. Angle (degrees)	Max. F_{Gn} (N)	Min. Angle (degrees)	Max. Angle (degrees)	Max. F_{Gn} (N)
Hui				-50.4±0.63	35.8±0.72	925.4±32.6
Iggy	-57.3±0.98	31.6±0.38	924.8±30.1			
Jie				-53.9±0.63	34.8±0.79	915.4±73.6
Kang	-55.0±0.59	34.0±0.62	932.9±21.4			

Table 2 summarises the measured oar angles and gate normal forces for this simulation.

The maximum gate normal forces were reduced by 1.6% (using kloss = 0.016) to bring the predicted mean hull velocity in line with the measured mean. The small decrease is considered to be justifiable given the standard deviations for the mean maximum forces shown in Table 4 and because of the uncertainties regarding temperature and wind speed.

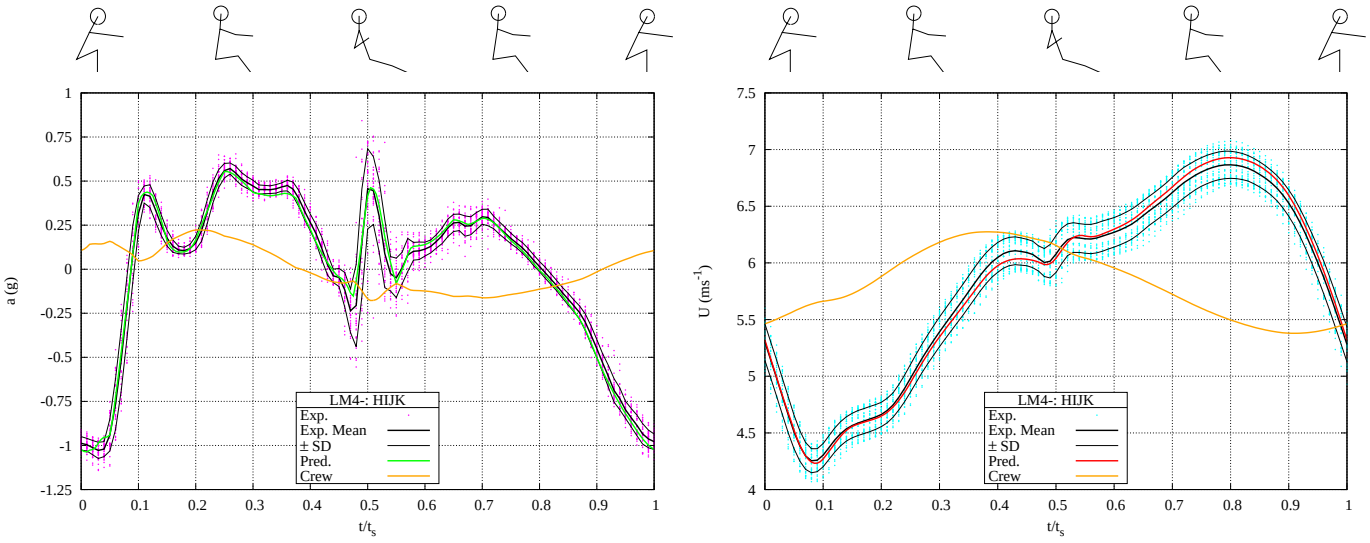

Figure 1: Hull propulsive acceleration and crew cg acceleration (left); hull velocity and crew cg velocity (right).

The hull propulsive acceleration is shown in the left panel of Fig. 1. Experimental data is shown as pink dots; the thick black curve is the mean of the measured values and the thin lines are one standard deviation (SD) either side of the mean curve. The green curve is FIRM's prediction.

Hull propulsive velocity and the speed of the crew CG is shown in the plot at the right of Fig. 1.

The forces in the equations of motion are shown in the left panel of Fig. 2. Drag components during the stroke are in the panel at the right.

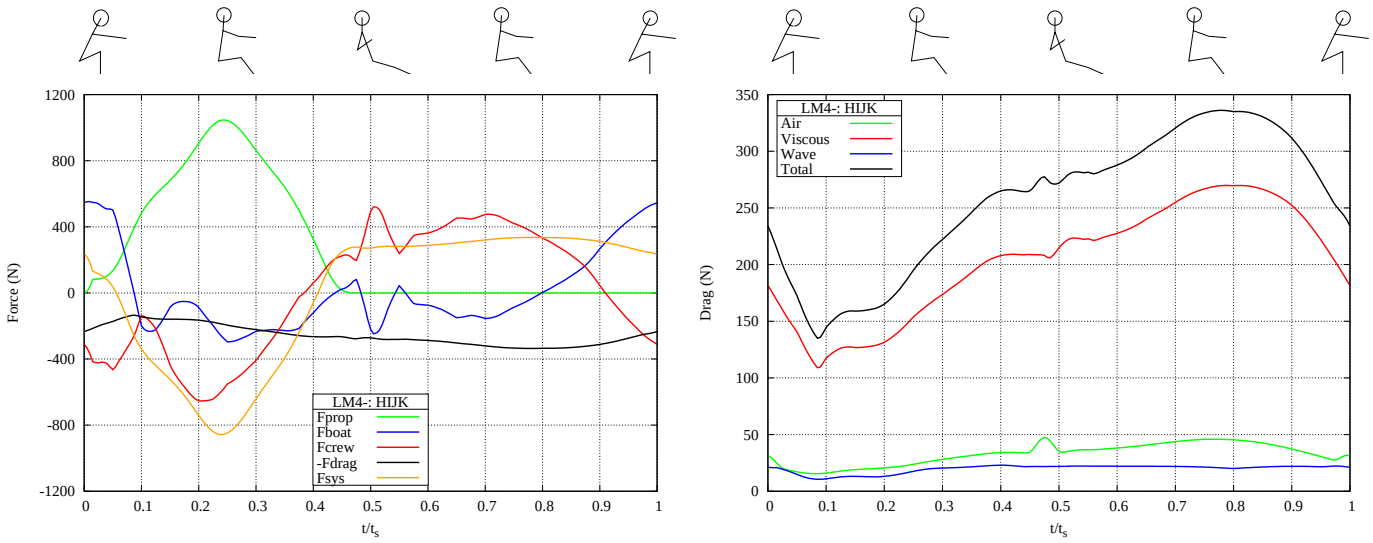

Figure 2: Equation of motion forces (left) and drag components (right).

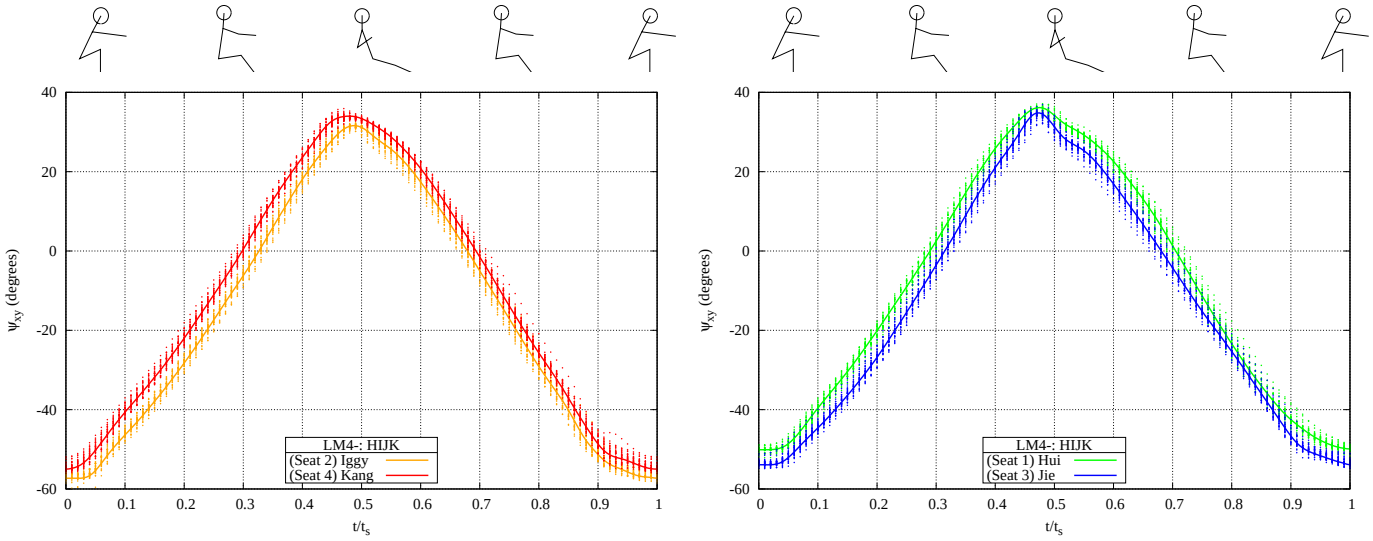

Figure 3: Oar azimuth angles Ψ_{xy}: Port side (left); Starboard side (right).

Experimental oar azimuth angles and values used as input to FIRM are shown in the two parts of Fig. 3.

Experimental gate normal forces and values used as input to FIRM are shown in the two parts of Fig. 4.

Blade propulsive forces are shown in the two parts of Fig. 5.

Dynamic oar lever ratios shown in Fig. 6 include the effect of variations in the location of the OBCP during the stroke.

Body angle regimes for two crew members are shown in the two parts of Fig. 7. The angles are the same for both crew members in this simulation.

Yawing moment lever arms and yawing moments are shown in the two parts of Fig. 8.

The OBCP trajectories in Fig. 9 have been plotted on the same side of the hull for clarity and comparison.

The OBCP trajectories in the yz-plane are shown in Fig. 10. For the purposes of this plot, the OBCP is assumed to be at the geometric centre of the blade when it is out of the water.

The OBCP is below the water from about $t/t_s = 0.01$ to $t/t_s \approx 0.47$. The latter value is the value entered in the main input file.

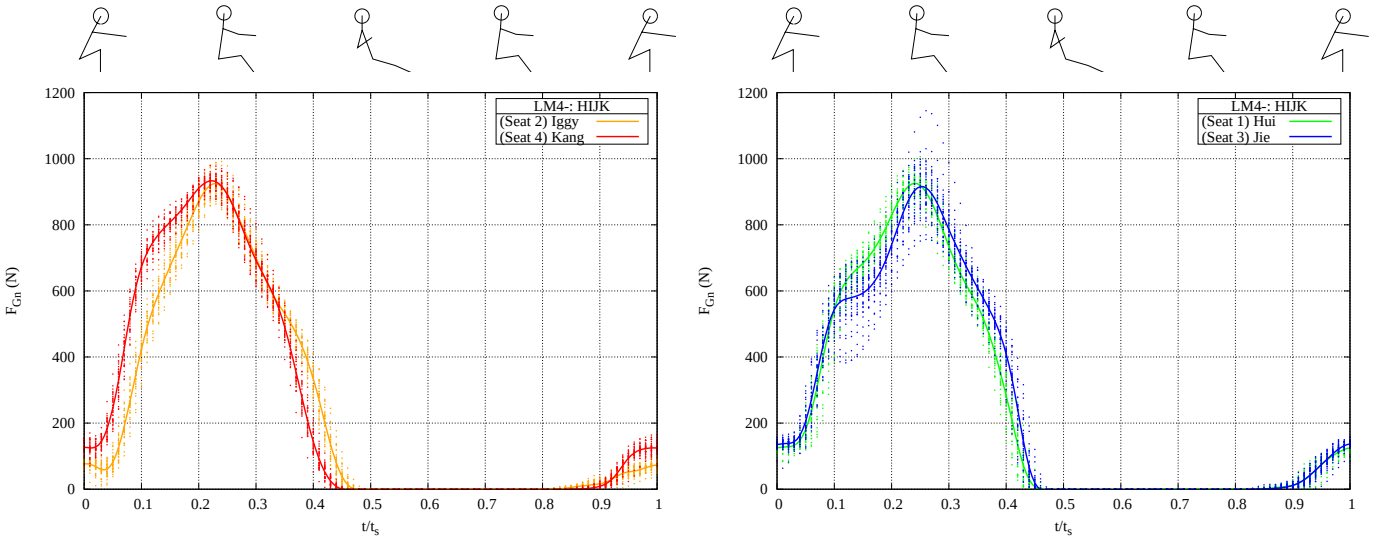

Figure 4: Gate normal forces F_{Gn}: Port side (left); Starboard side (right).

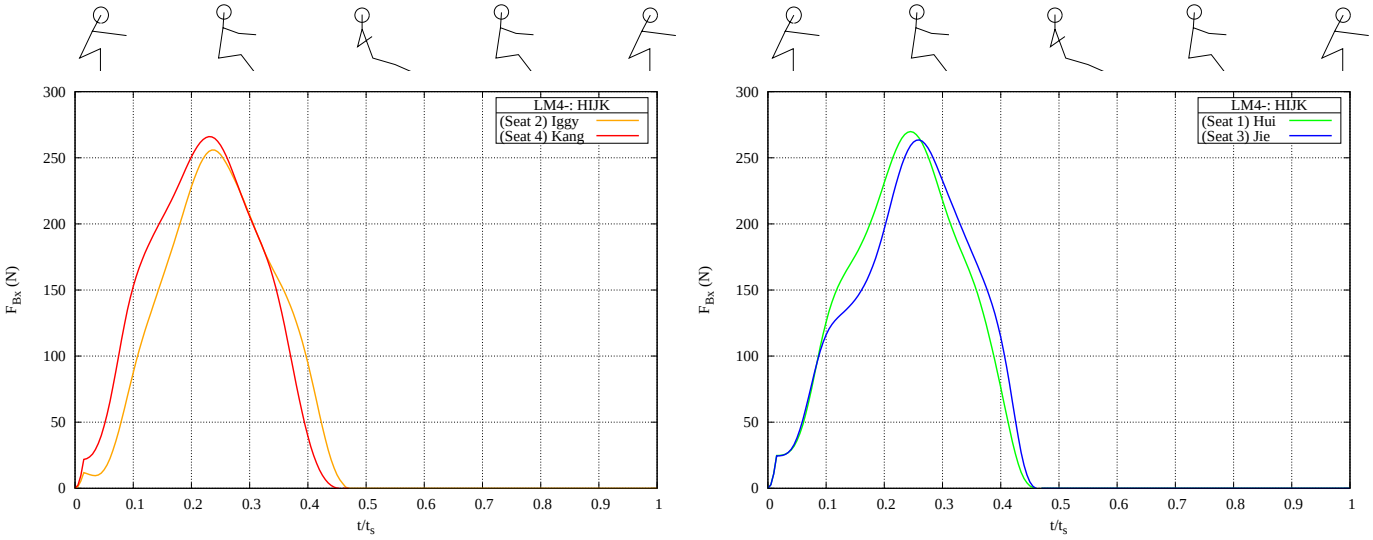

Figure 5: Blade propulsive forces F_{Bx}: Port side (left); Starboard side (right).

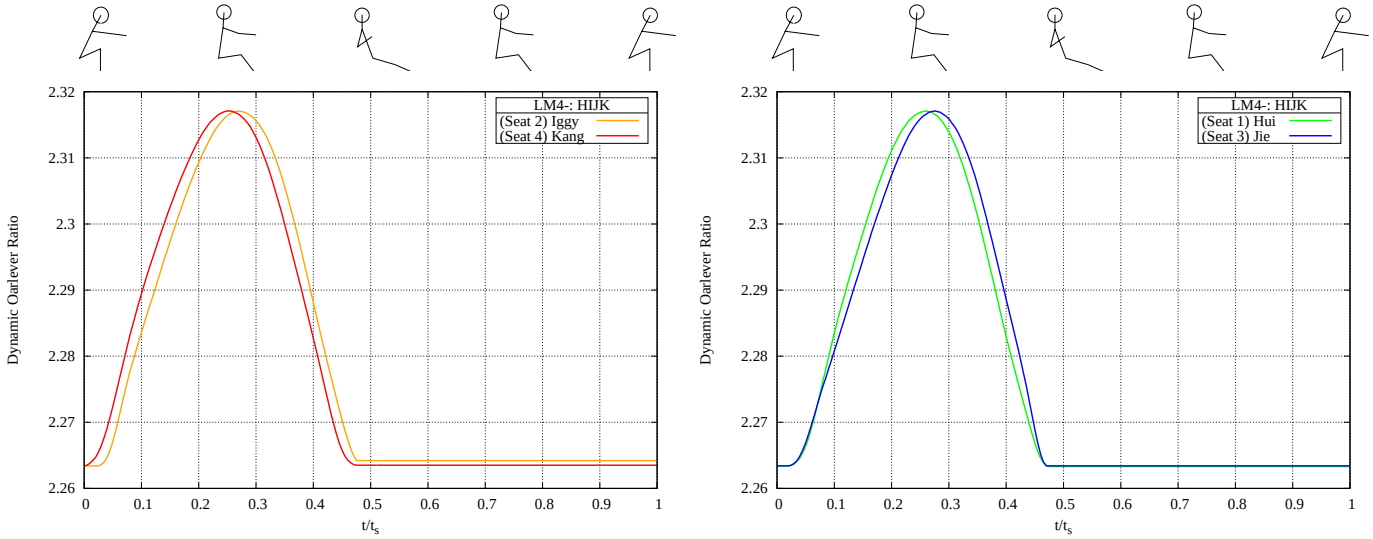

Figure 6: Dynamic oarlever ratios: Port side (left); Starboard side (right).

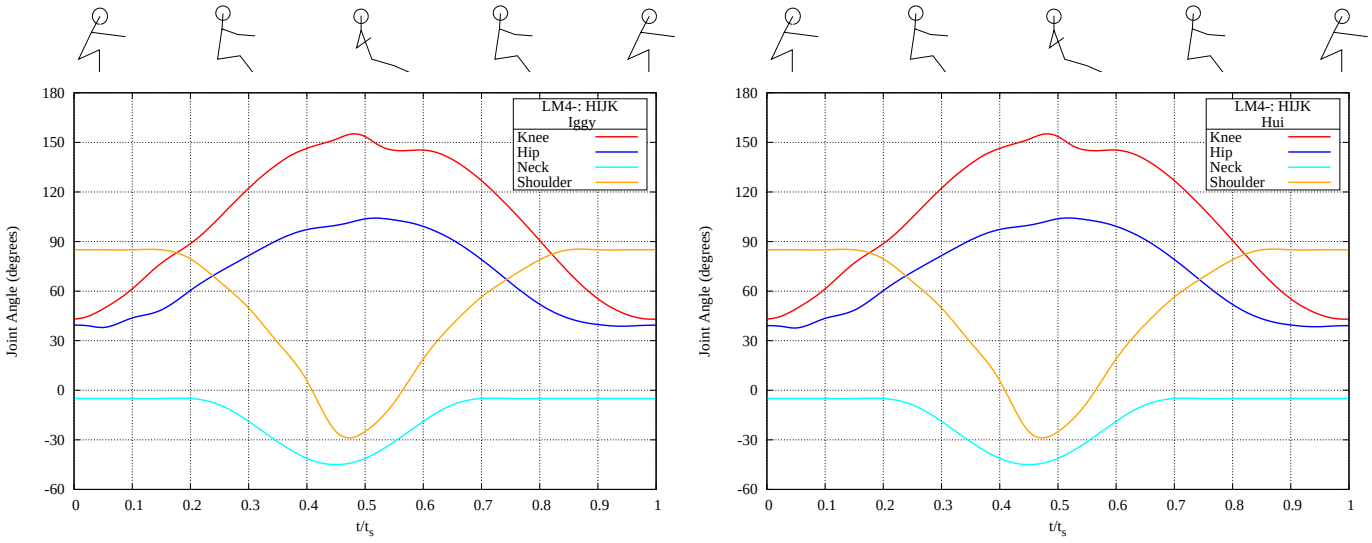

Figure 7: Joint angles: Seat 2 (left): Seat 1 (right).

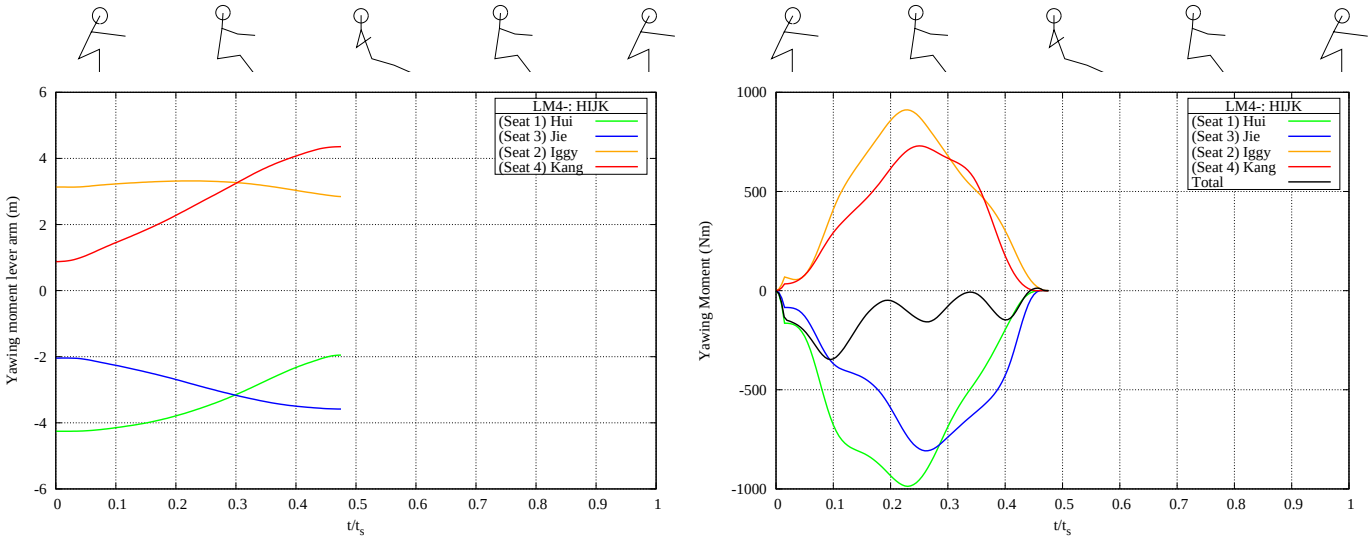

Figure 8: Yawing moment lever arms L_{yaw} (left); yawing moments M_{yaw} (right).

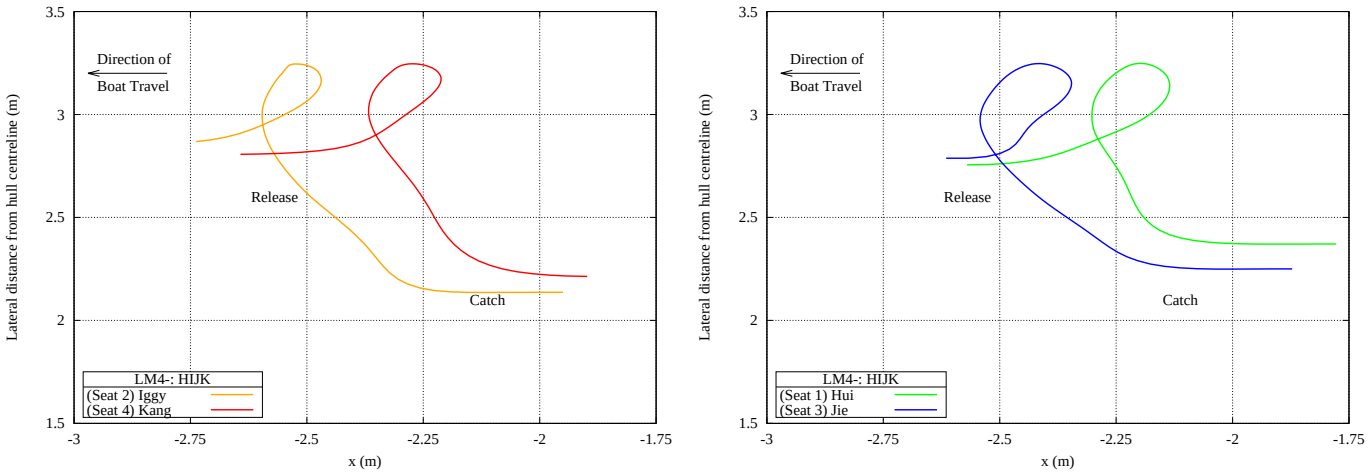

Figure 9: OBCP trajectories in the xy-plane: Port side (left); Starboard side (right).

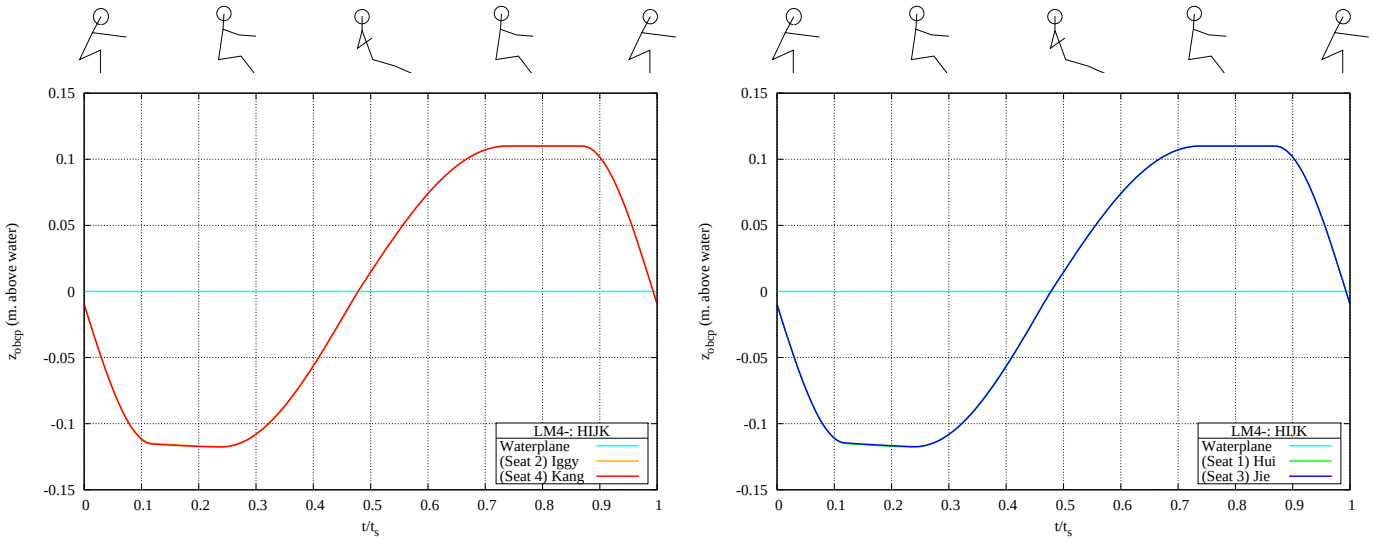

Figure 10: OBCP trajectories in the yz-plane: Port side (left); Starboard side (right).

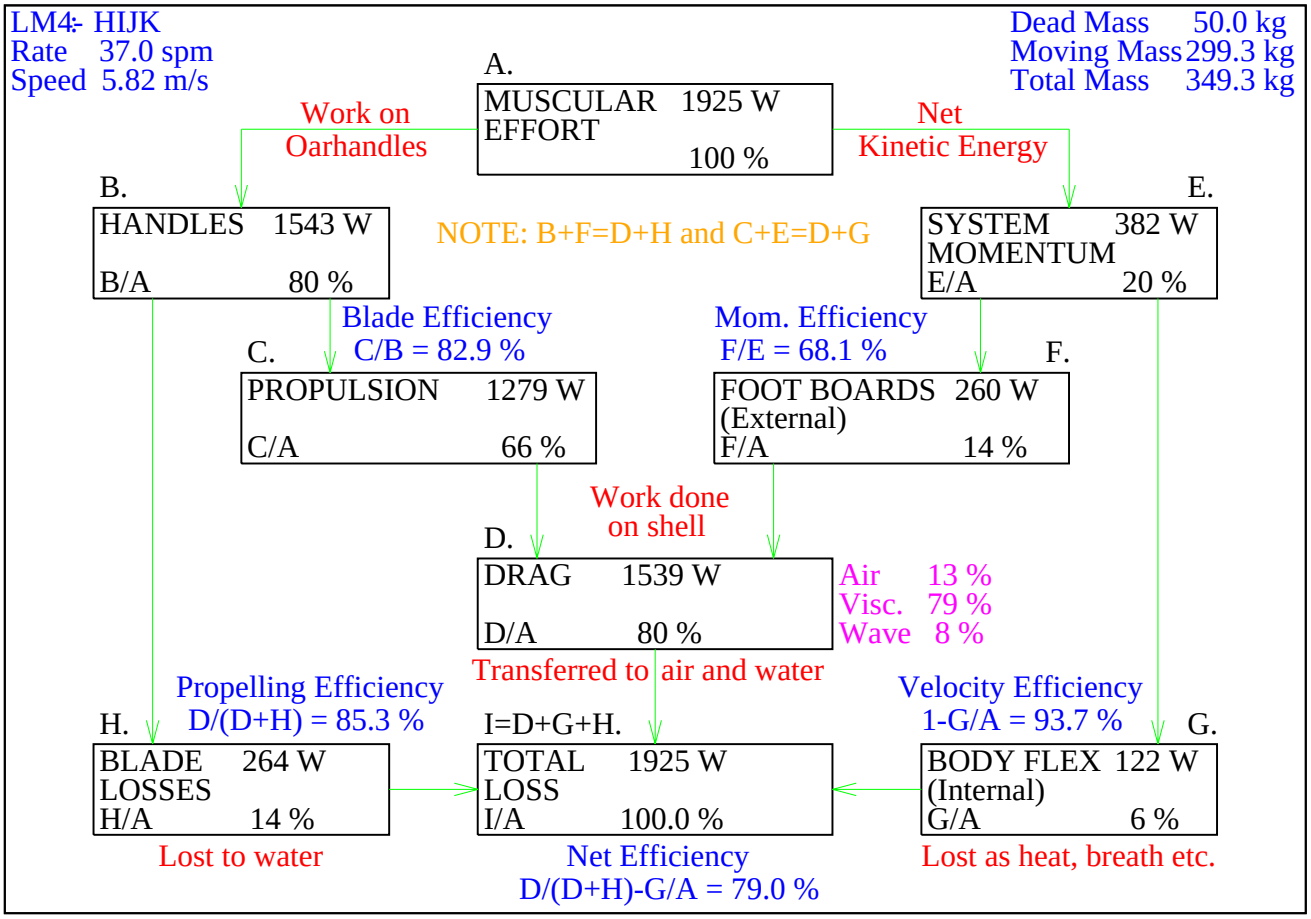

Figure 11: Power flow chart.

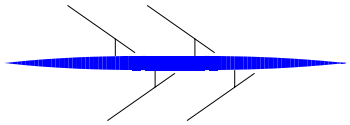

3 M4-: Men's Four (Normal Rig)

The on-water trial for this men's four, "Yuri", "Conan", "Dazza" and "Zeke", was conducted over 2000m on a mid-winter morning. Air and water temperatures were not recorded: they were estimated as 11°C and 11°C respectively. Measured values of rigging details, oar angles, gate normal forces, and their anthropometry were used as input to FIRM. Body angle regimes were not recorded but were estimated by the author using a complicated fitting process.

Table 3: Summary of experimental results for this simulation: number of strokes, stroke rate, non-dimensional pull phase duration (t_p/t_s), minimum hull velocity (U_{min}), maximum hull velocity (U_{max}), and mean hull velocity ($\overline{U}$).

Item	Value
Nstrokes	38
Rate (spm)	37.789 ±0.317
t_p/t_s	0.518 ±0.011
U_{min} (ms^{-1})	3.956 ±0.049
U_{max} (ms^{-1})	6.728 ±0.073
$\overline{U}$ (ms^{-1})	5.523 ±0.055

Table 3 summarises the main quantities relating to the simulation for this crew. Values are given ± one standard deviation.

Table 4: Experimental oar-related values for this simulation: Minimum and maximum oar angles, and maximum gate normal force.

Name	Port Oar			Starboard Oar		
	Min. Angle (degrees)	Max. Angle (degrees)	Max. F_{Gn} (N)	Min. Angle (degrees)	Max. Angle (degrees)	Max. F_{Gn} (N)
Yuri				-53.4±0.58	30.7±0.54	822.8±37.1
Conan	-54.4±0.58	31.4±0.37	935.9±36.8			
Dazza				-51.2±0.70	32.5±0.35	836.0±40.7
Zeke	-51.0±0.59	34.9±0.42	1092.9±54.0			

Table 4 summarises the measured oar angles and gate normal forces for this simulation.

The maximum gate normal forces were decreased by 2.1% (using kloss = 0.02) to bring the predicted mean hull velocity in line with the measured mean. The small decrease is considered to be justifiable given the standard deviations for the mean maximum forces shown in Table 4 and because of the uncertainties regarding temperature and wind speed.

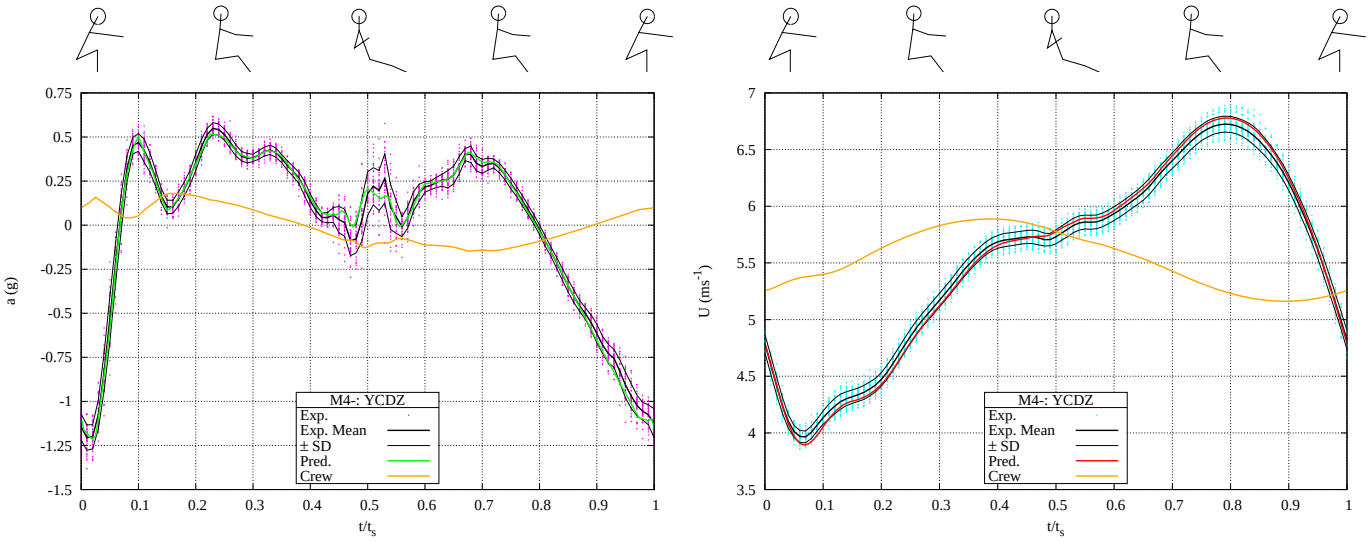

Figure 12: Hull propulsive acceleration and crew cg acceleration (left); hull velocity and crew cg velocity (right).

The hull propulsive acceleration is shown in the left panel of Fig. 12. Experimental data is shown as pink dots; the thick black curve is the mean of the measured values and the thin lines are one standard deviation (SD) either side of the mean curve. The green curve is FIRM's prediction.

Hull propulsive velocity and the speed of the crew CG is shown in the plot at the right of Fig. 12.

The forces in the equations of motion are shown in the left panel of Fig. 13. Drag components during the stroke are in the panel at the right.

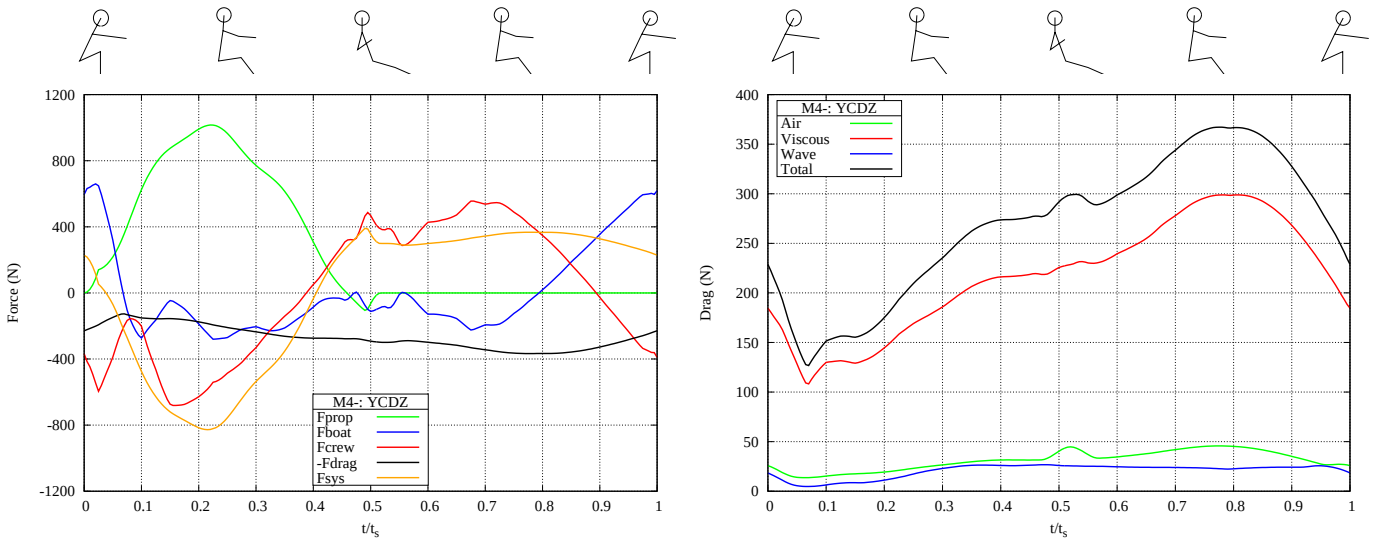

Figure 13: Equation of motion forces (left) and drag components (right).

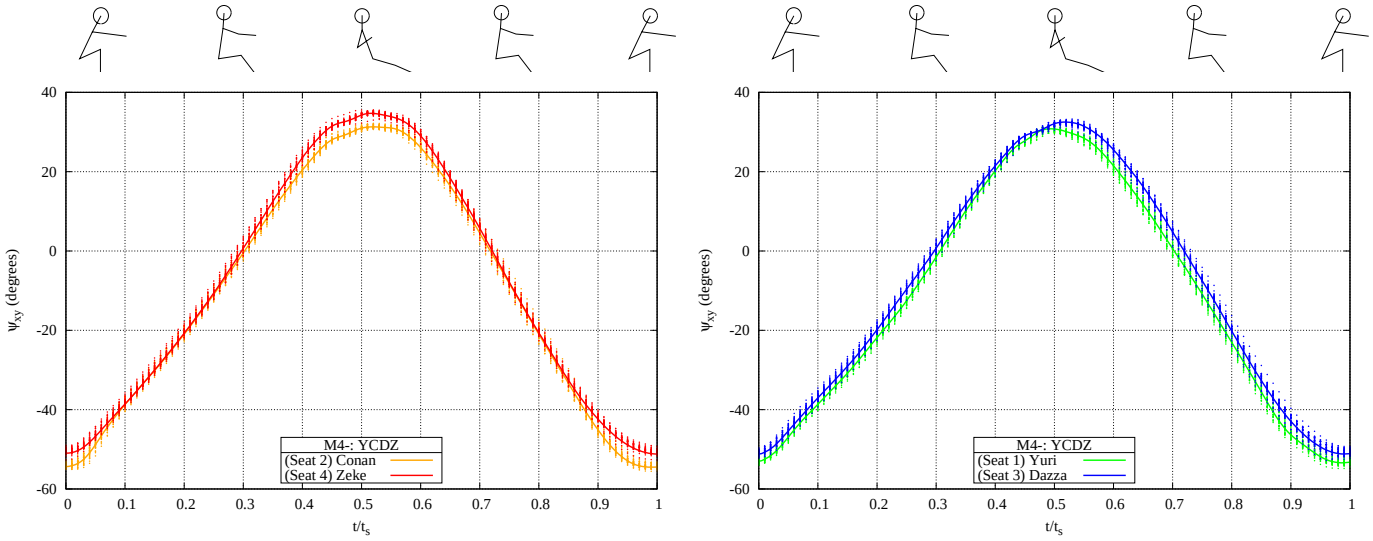

Figure 14: Oar azimuth angles Ψ_{xy}: Port side (left); Starboard side (right).

Experimental oar azimuth angles and values used as input to FIRM are shown in the two parts of Fig. 14.

Experimental gate normal forces and values used as input to FIRM are shown in the two parts of Fig. 15.

Blade propulsive forces are shown in the two parts of Fig. 16.

Dynamic oar lever ratios shown in Fig. 17 include the effect of variations in the location of the OBCP during the stroke.

Body angle regimes for two crew members are shown in the two parts of Fig. 18. The angles are the same for all crew members in this simulation. Differences in hip angles are due to slight differences in feet heights and limb lengths.

Yawing moment lever arms and yawing moments are shown in the two parts of Fig. 19.

The OBCP trajectories in Fig. 20 have been plotted on the same side of the hull for clarity and comparison.

The OBCP trajectories in the yz-plane are shown in Fig. 21. For the purposes of this plot, the OBCP is assumed to be at the geometric centre of the blade when it is out of the water.

The OBCP is below the water from about $t/t_s = 0.01$ to $t/t_s \approx 0.518$. The latter value is the value entered in the main input file.

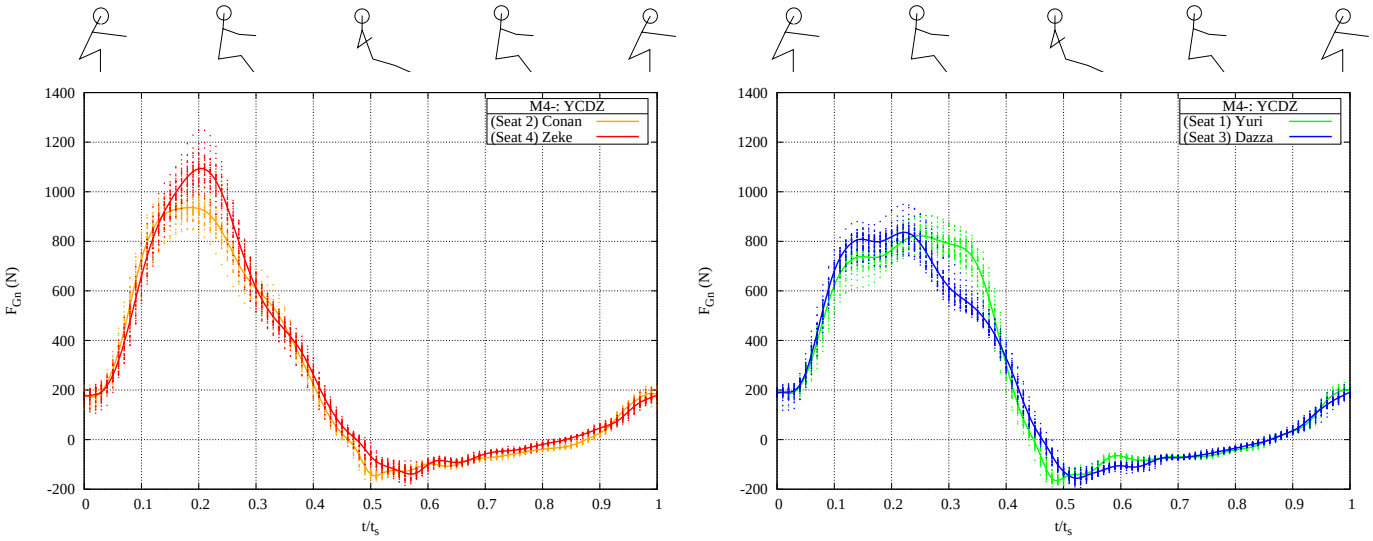

Figure 15: Gate normal forces F_{Gn}: Port side (left); Starboard side (right).

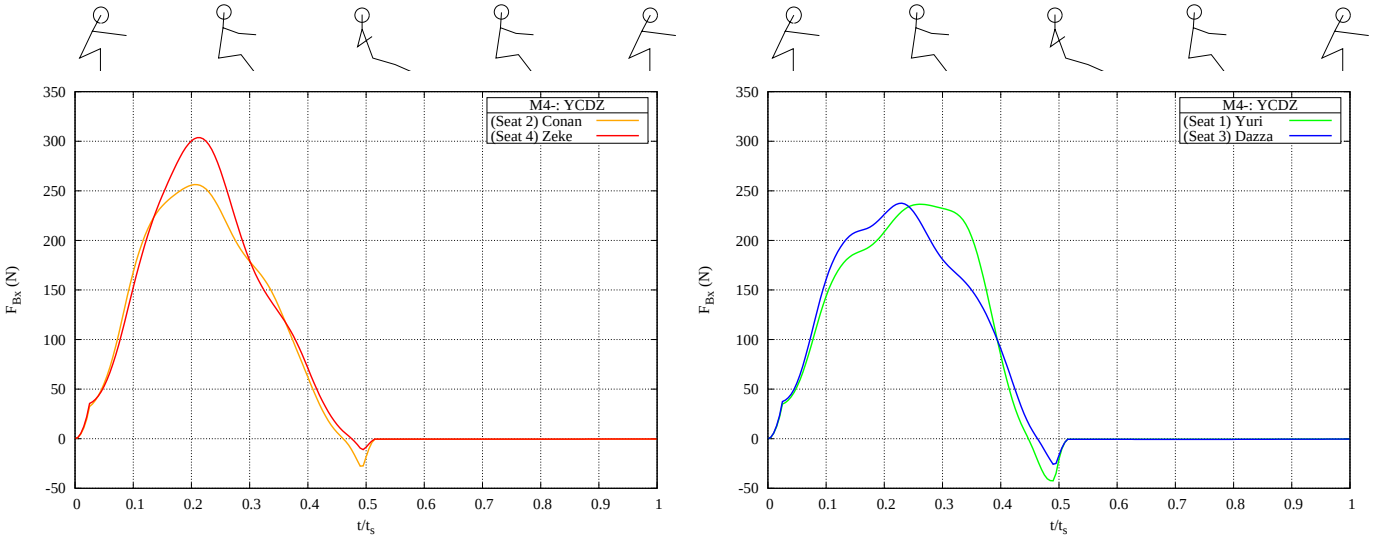

Figure 16: Blade propulsive forces F_{Bx}: Port side (left); Starboard side (right).

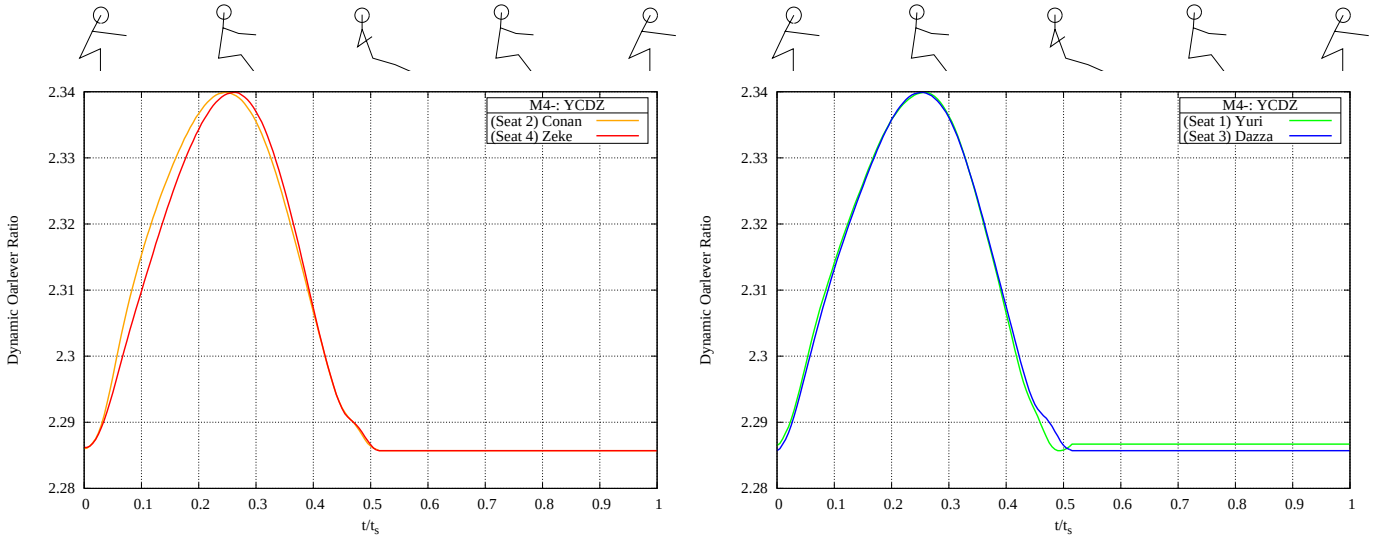

Figure 17: Dynamic oarlever ratios: Port side (left); Starboard side (right).

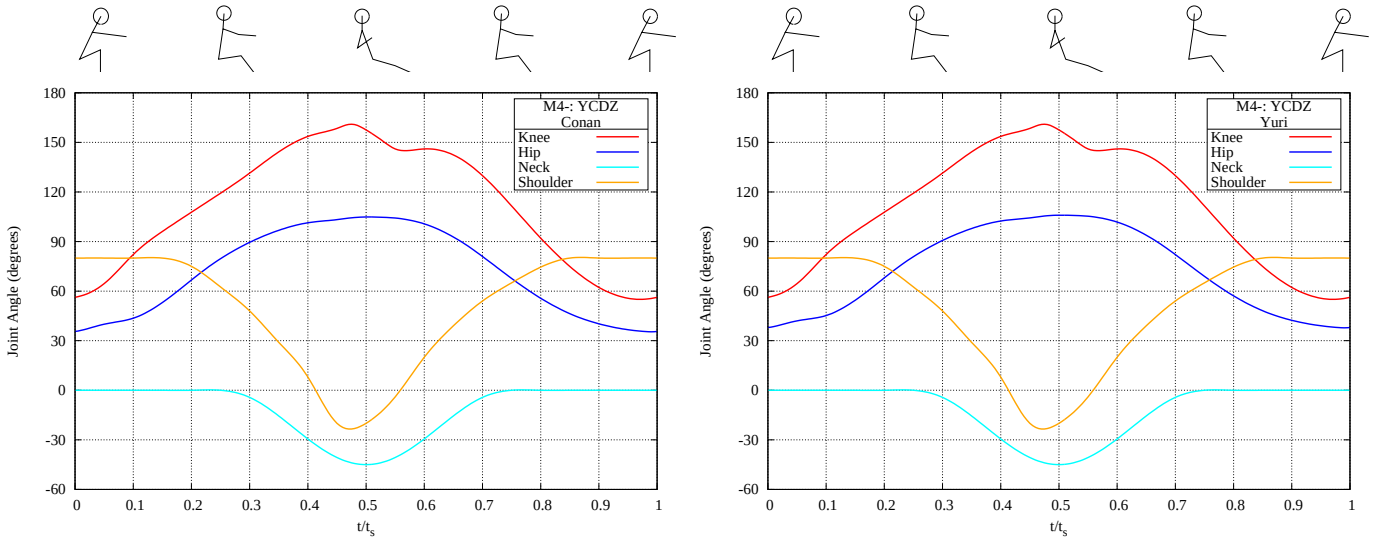

Figure 18: Joint angles: Seat 2 (left): Seat 1 (right).

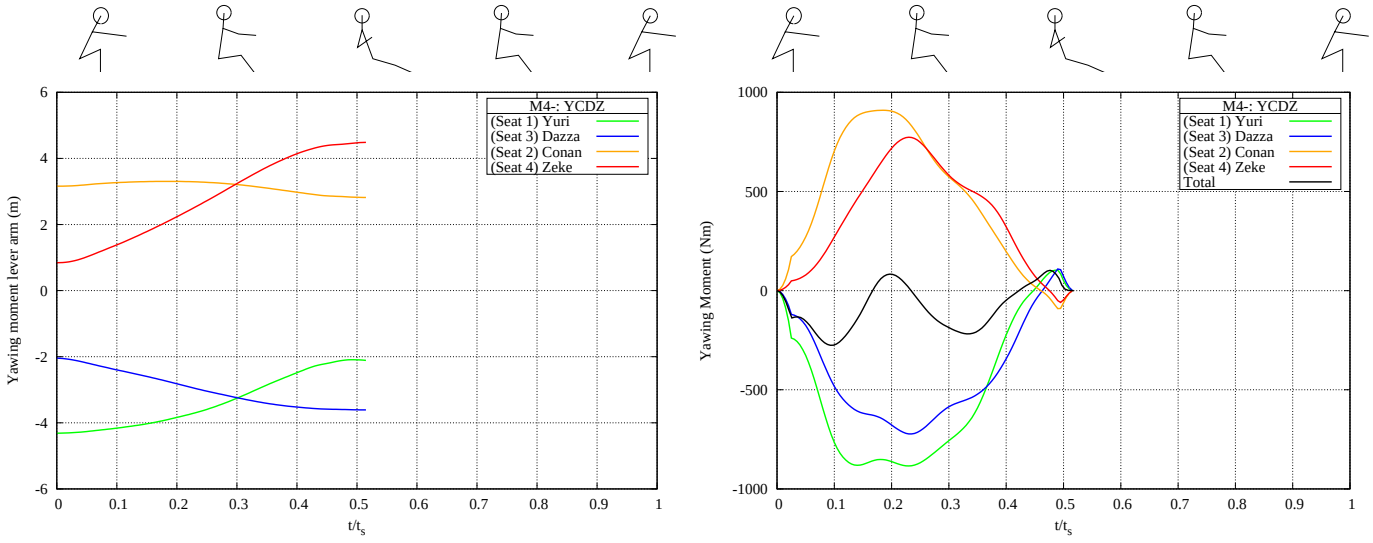

Figure 19: Yawing moment lever arms L_{yaw} (left); yawing moments M_{yaw} (right).

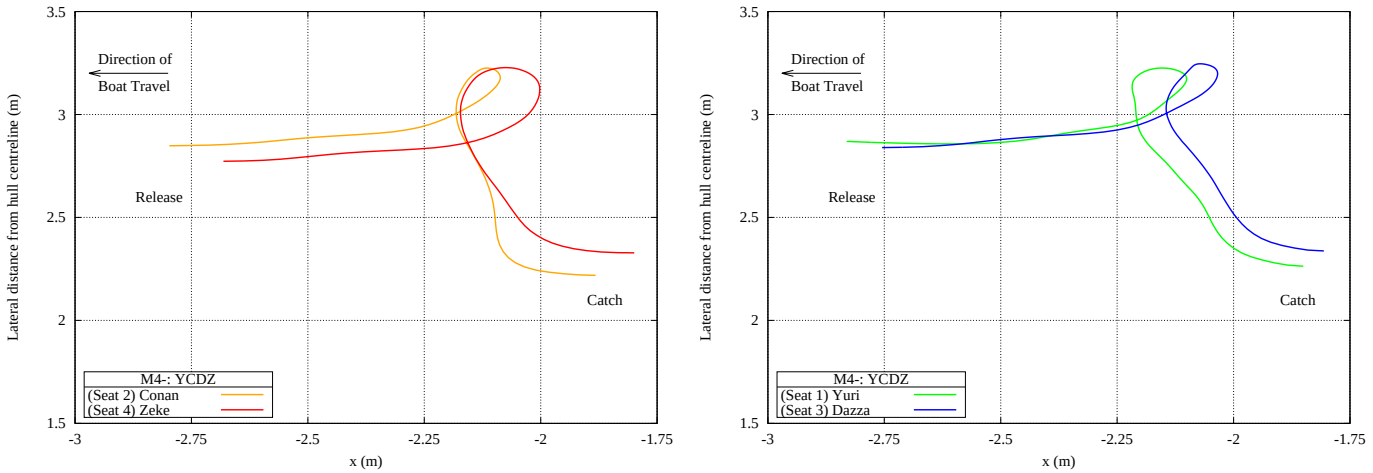

Figure 20: OBCP trajectories in the xy-plane: Port side (left); Starboard side (right).

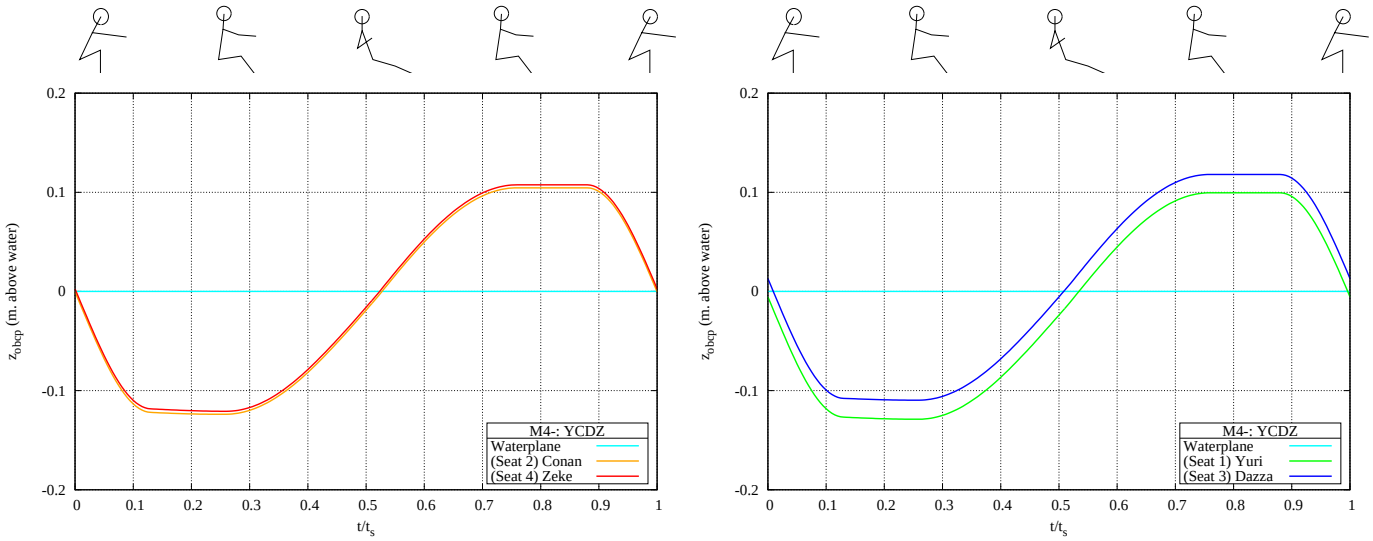

Figure 21: OBCP trajectories in the yz-plane: Port side (left); Starboard side (right).

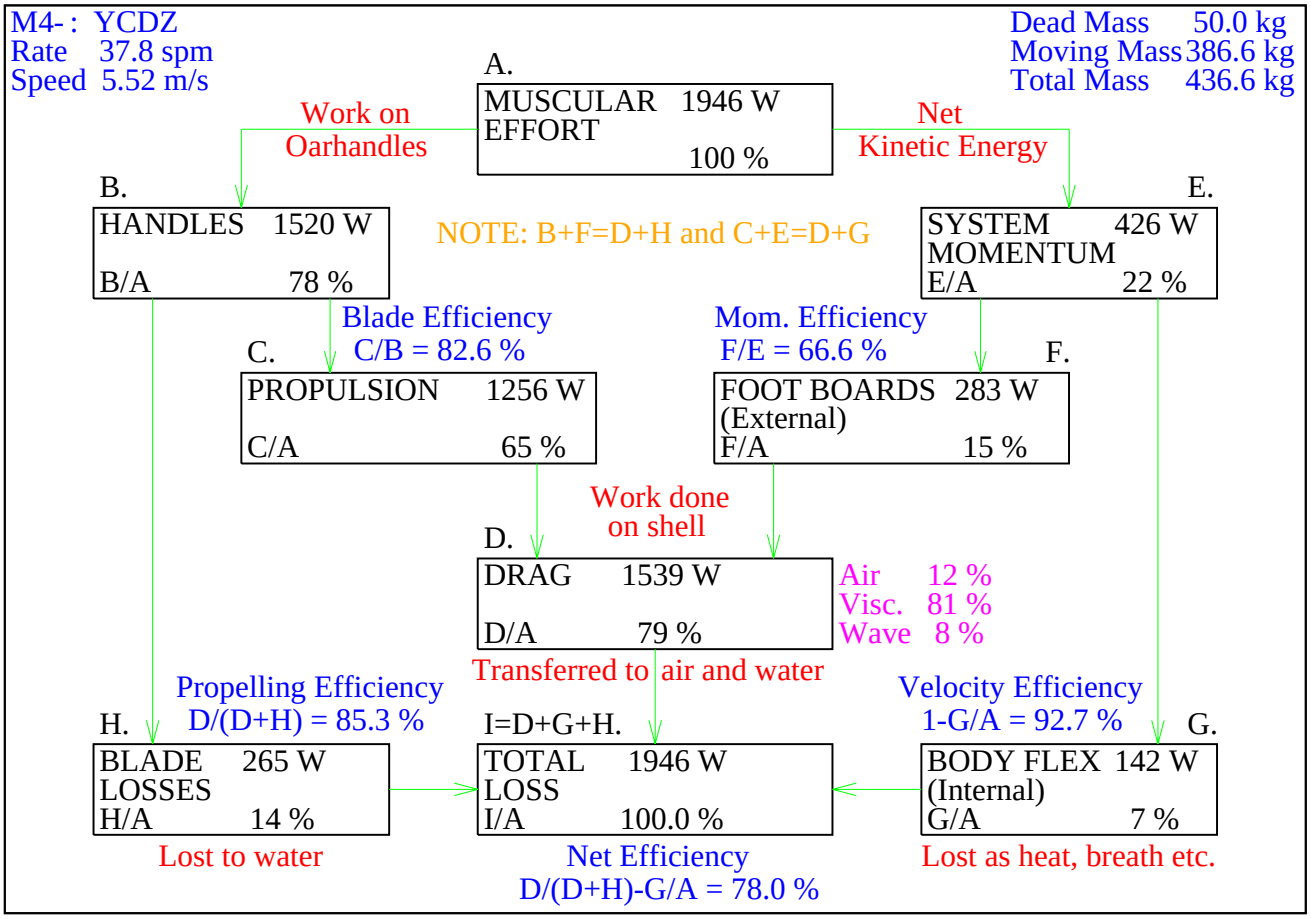

Figure 22: Power flow chart.

3.1 M4-: Men's Four (Italian Rig)

This example uses many of the same input files as the M4- example in Section 3. To run the example double-click on the icon for the batch file m4m_cydz_italian.bat.

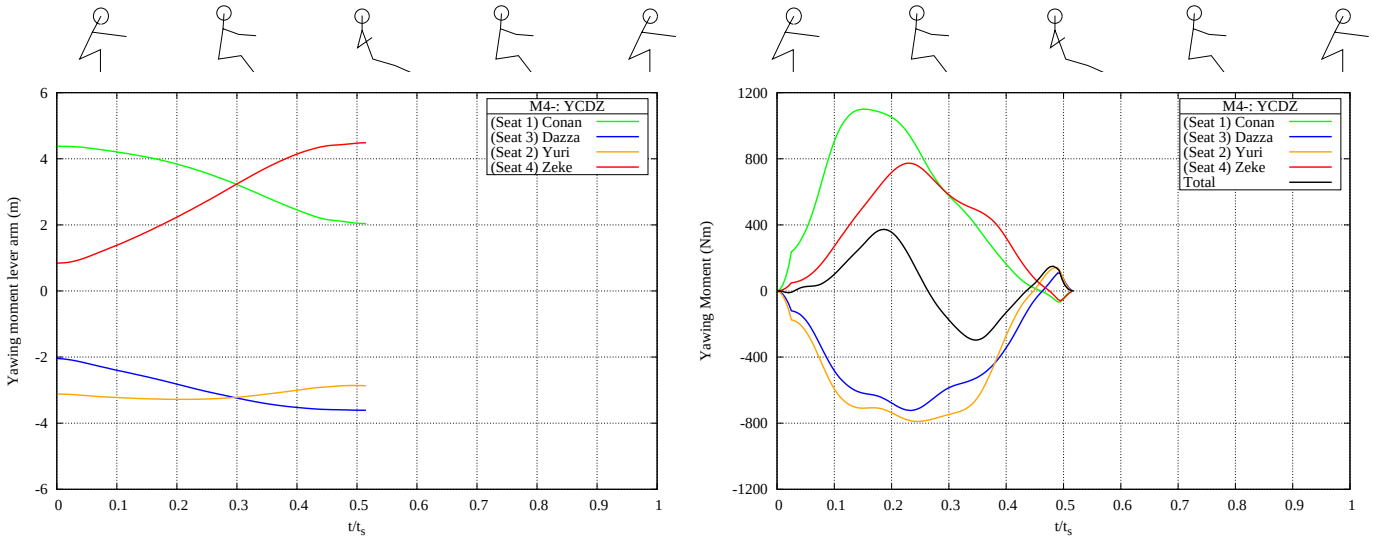

Figure 23: Yawing moment lever arms L_{yaw} (left); yawing moments M_{yaw} (right).

Yawing moment lever arms and yawing moments are shown in the two parts of Fig. 23.

This arrangement of oars produces a relatively large positive yawing moment for the first part of the drive phase, which tends to move the bow to the port side of the boat. During the latter part of the drive phase the nett yawing moment is negative, which would tend to move the bow back towards the starboard side.

3.2 M4-: Men's Four (Clones)

To run this example double-click on the icon for the batch file m4m_clones.bat.

The rowers are all clones of Yuri. The only difference from the "real" Yuri, is that two of the clones row on the port side of the boat.

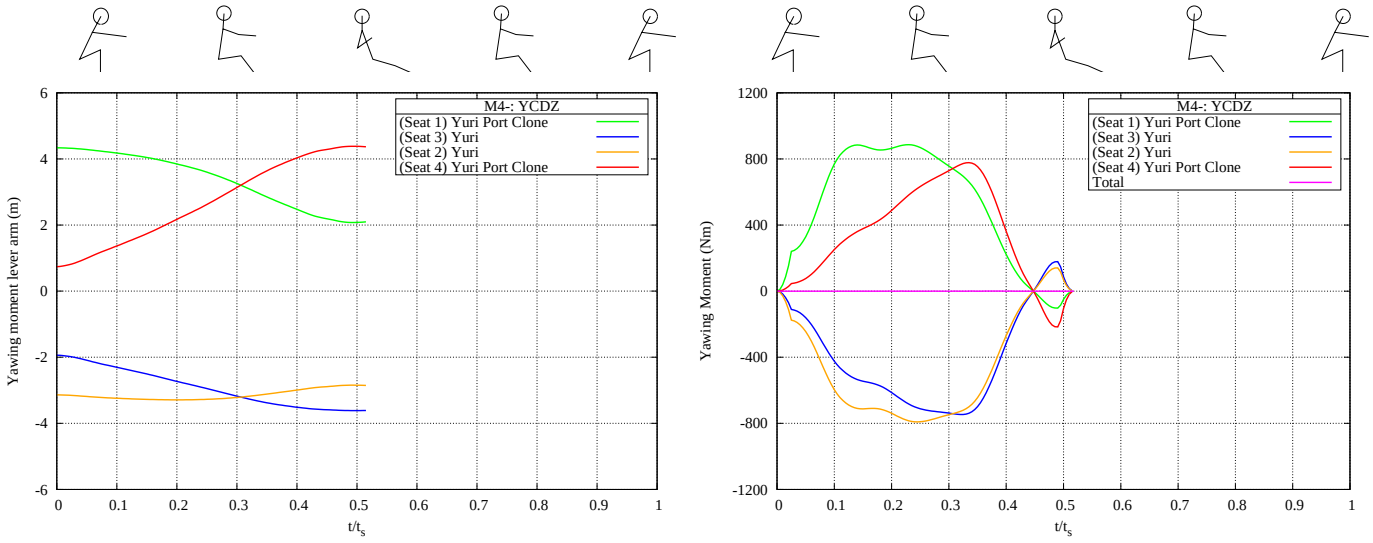

Figure 24: Yawing moment lever arms L_{yaw} (left); yawing moments M_{yaw} (right).

Yawing moment lever arms and yawing moments are shown in the two parts of Fig. 24.

Although the individual yawing moments produced by each oar are non-zero, their sum is zero, which constitutes one verification that FIRM is operating correctly.

3.3 M4-: Mens' Four (Worst Rig)

This example uses many of the same input files as the M4- (Normal Rig) example in Section 3 and the Italian Rig example in Section 3.1. To run the example double-click on the icon for the batch file m4m_ydcz_worst.bat.

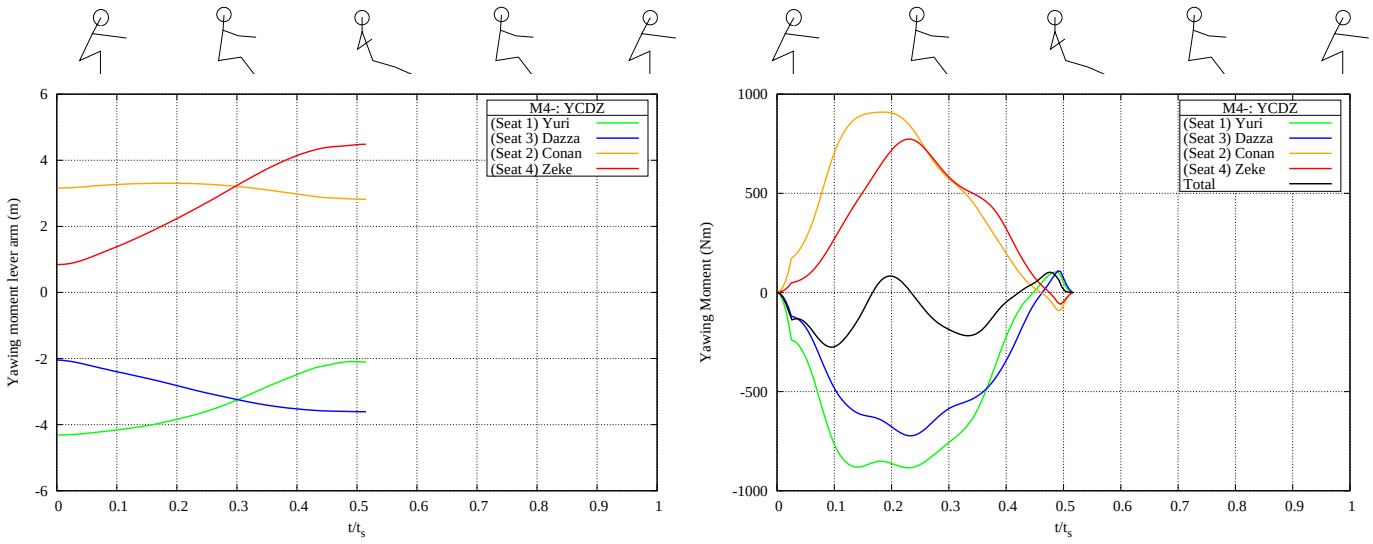

Figure 25: Yawing moment lever arms L_{yaw} (left); yawing moments M_{yaw} (right).

Yawing moment lever arms and yawing moments are shown in the two parts of Fig. 25.

This arrangement of oars produces a large nett negative yawing moment which tends to move the bow to the starboard side of the boat for most of the stroke.

3.4 M4-: Men's Four Rig Comparisons

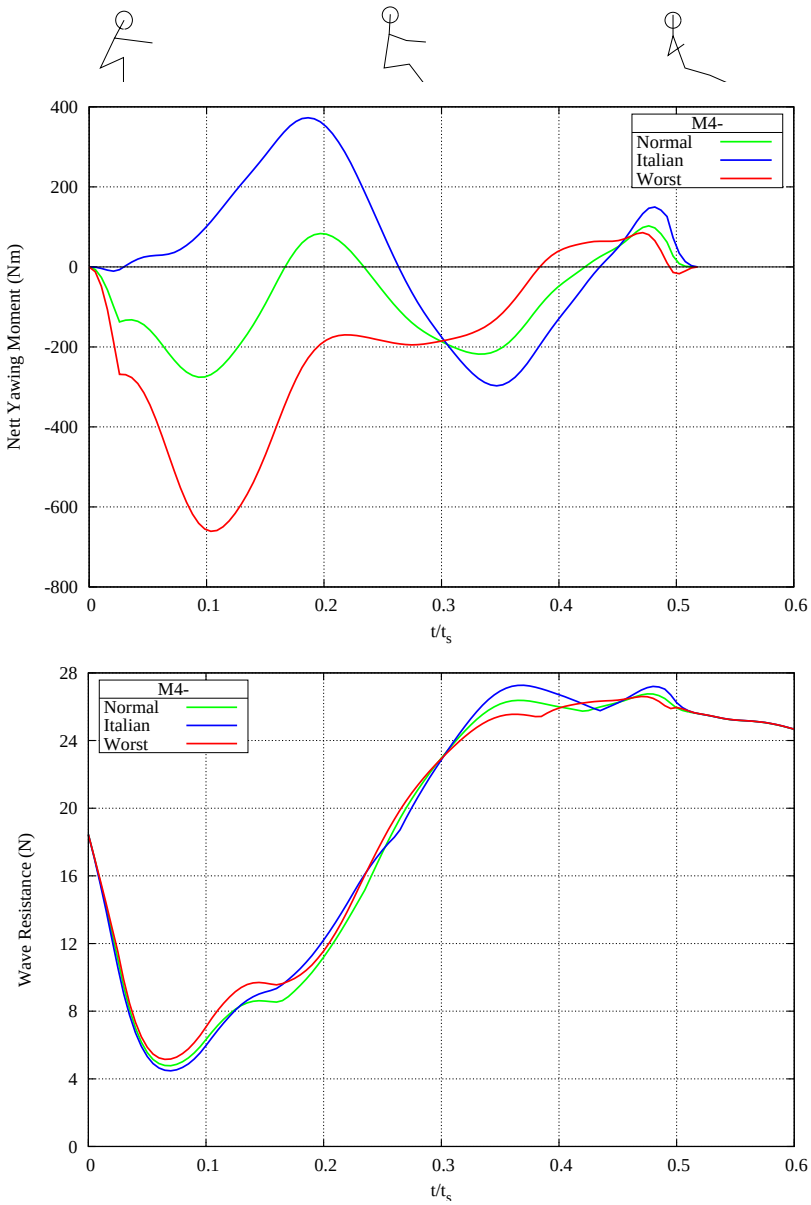

Figure 26: Nett yawing moment (top) and wave resistance (bottom) of three men's fours rigs.

Fig. 26 shows the total nett yawing moment and the wave resistance of the three rigs for men's fours in Sections 3, 3.1 and 3.3. For greater clarity results are shown only for the drive phase. Moments are equal to zero for the recovery phase, and there is no effect of yawing on resistance.

The nett yawing moment for the Normal Rig is negative for the first half of the drive phase. This tends to push the bow to starboard. At square-off the yawing moment becomes slightly positive, which tends to push the bow back to port. After square-off the moment again becomes negative and then drops back towards zero. The nett effect is that the bow will tend to be pushed towards the starboard side of the boat and some rudder correction will need to be applied.

For the Italian Rig, the yawing moment is large and positive before square-off. It then decays down to zero at about square-off, after which it then becomes negative at about $t/t_s = 0.35$ before returning towards zero at the end of the drive. The nett effect is that a smaller rudder correction will need to be applied than for the Normal Rig.

The Worst Rig produces a large negative yawing moment at $t/t_s = 0.1$ which will push the bow towards the starboard side of the boat. The moment then decays back towards zero at the end of the drive phase. The nett effect is that a large rudder correction will need to be applied.

The effect of yawing moments on the wave resistance is shown in the plot at the bottom of Fig. 26. It can be seen that wave resistance is higher for those instants where the absolute value of the yawing moment is greatest. However, the differences between the three rigs is, at most, only of the order of about one Newton.